JGR Atmospheres

RESEARCH ARTICLE
10.1029/2022JD037727

The Contribution of Subtropical Moisture Within an Atmospheric River on Moisture Flux, Cloud Structure, and Precipitation Over the Salmon River Mountains of Idaho Using Moisture Tracers

Divya Rea[1], Robert M. Rauber[1], Huancui Hu[2], Sarah A. Tessendorf[3], Steve W. Nesbitt[1], Brian F. Jewett[1], and Troy J. Zaremba[1]

[1]Department of Atmospheric Sciences, University of Illinois Urbana-Champaign, Urbana, IL, USA, [2]Pacific Northwest National Laboratory, Richland, WA, USA, [3]National Center for Atmospheric Research, Boulder, CO, USA

Key Points:

- The water vapor tracing tool within WRF permits a better understanding of the impact of atmospheric rivers (ARs) on the interior mountains
- During this AR, the tropospheric moisture flux across the mountains of Idaho was primarily subtropical moisture advected by the AR
- In this case, precipitation attributable to subtropical moisture advected by the AR ranged from 35 (northern Idaho) to 90% (southern Idaho)

Correspondence to:
D. Rea,
dprea2@illinois.edu

Citation:
Rea, D., Rauber, R. M., Hu, H., Tessendorf, S. A., Nesbitt, S. W., Jewett, B. F., & Zaremba, T. J. (2023). The contribution of subtropical moisture within an atmospheric river on moisture flux, cloud structure, and precipitation over the Salmon River Mountains of Idaho using moisture tracers. *Journal of Geophysical Research: Atmospheres*, *128*, e2022JD037727. https://doi.org/10.1029/2022JD037727

Received 24 AUG 2022
Accepted 27 FEB 2023

Author Contributions:
Conceptualization: Divya Rea, Robert M. Rauber
Formal analysis: Divya Rea
Funding acquisition: Robert M. Rauber
Methodology: Divya Rea, Huancui Hu, Steve W. Nesbitt, Brian F. Jewett, Troy J. Zaremba
Software: Troy J. Zaremba
Writing – original draft: Divya Rea
Writing – review & editing: Robert M. Rauber, Huancui Hu, Sarah A. Tessendorf, Steve W. Nesbitt, Brian F. Jewett, Troy J. Zaremba

Abstract The impact of an atmospheric river (AR) on the flux of subtropical moisture across Idaho's Salmon River Mountains and precipitation over the mountains is evaluated using the Weather, Research, and Forecasting model with water vapor tracers (WRF-WVT). The AR impacted Idaho between 17 and 19 January 2017 during the Seeded and Natural Orographic Wintertime Clouds: The Idaho Experiment (SNOWIE) campaign. WRF-WVT is configured to isolate the subtropical moisture contribution to the AR, the moisture flux, and precipitation. Subtropical water vapor advected by the AR into Idaho is tagged and tracked in three-dimensional space throughout the run. This allows the contribution of the subtropical moisture to the vertical distribution of water vapor and the precipitation to be directly calculated. The simulated cloud structure is compared with airborne radar data collected during two SNOWIE intensive operation periods. This study found that more than 70% of the moisture flux and more than 80% of the precipitation across the Idaho Mountains during SNOWIE IOP 4 could be attributed to subtropical moisture within the AR. Nearly all of the moisture flux in the upper cloud and 50% of the moisture in the lower cloud was attributable to the subtropical moisture. The subtropical moisture contribution within the AR to precipitation ranged from 35% in northern Idaho to more than 90% in southern Idaho. Across the entire period of impact of the AR, more than 60% of precipitation in Idaho was attributable to the subtropical moisture within the AR, with this percentage increasing toward the south across the state.

Plain Language Summary Atmospheric rivers (ARs) are streams of strong moisture transport that often form along and ahead of the cold front of extratropical cyclones. They often bring heavy precipitation to the U.S. west coast resulting in hazardous conditions and flooding. States like Idaho are dependent on ARs for snowpack enhancement to prevent water shortages and support the creation of hydroelectric power. ARs often draw moisture into the west coast from the tropics and subtropics. This analysis presents a case study showing how the moisture flux from subtropical latitudes associated with an AR varied over Idaho's Salmon River Mountains during the course of several days. This analysis traced water vapor that originated south of 35°N within the AR. More than 60% of precipitation in Idaho during this event was directly attributable to subtropical moisture within the AR, with this percentage increasing toward the south across the state. This analysis also examines how subtropical moisture transport varied with depth within the troposphere over the Salmon River Mountains and how the moisture distribution impacted cloud structure, as measured by an airborne vertically pointing radar. This study contributes a better understanding of how Pacific ARs impact water resources over the mountains of Idaho.

1. Introduction

In the last decade, atmospheric rivers (ARs) have increasingly become a focus of research (Ralph et al., 2017; Shields et al., 2018). Guan and Waliser (2015) determined that around 11 ARs are detectable globally at any given time, transporting on average 374 kg m^{-1} s^{-1} of columnar water vapor. While only two or three ARs make landfall at any given time (Guan & Waliser, 2015), they often bring hazardous weather (Waliser & Guan, 2017). ARs have been studied most extensively along the west coast of the United States. Ninety percent of flooding events along the west coast have been attributed to ARs, as well as 20%–50% of California's annual precipitation (Cao et al., 2021; Dettinger et al., 2011).

Several studies have attempted to estimate the contribution of landfalling ARs to total winter precipitation over the intermountain western U.S. Dettinger et al. (2011) used data from two polar-orbiting satellites to identify the day of and day following the landfall of ARs on North America's west coast between 32.5° and 52.5°N. They combined this information with daily precipitation measurements from National Weather Service Cooperative Observer sites to estimate the contribution to total precipitation from ARs. They found that about 10%–40% of the total precipitation in Idaho could be attributed to ARs, with that value decreasing to less than 20% in Utah and less than 10% in other locations in the intermountain western U.S. (their Figure 6). Rutz and Steenburgh (2012) expanded the Dettinger et al. (2011) analysis, identifying ARs using six-hourly summaries of integrated water vapor (IWV) at 1.5° resolution from the ERA-Interim reanalysis, and included high-elevation Snowpack Telemetry (SNOTEL) stations and an expanded latitude range southward to 24°N, in order to quantify the role of ARs making landfall along Mexico's Baja Peninsula. Their results showed that less than ∼36% of high-altitude precipitation resulted from ARs in Idaho, reducing to 28% in Utah, and smaller amounts in other intermountain locations. Rutz et al. (2014) conducted a similar analysis to Rutz and Steenburgh (2012) but using six-hourly observations of integrated water vapor transport (IVT) instead of IWV, with the added constraint that precipitation was only attributed to ARs if AR conditions were met at the given location. They found that up to ∼30% of the precipitation in the southwest central Idaho Mountains was attributable to ARs, with this value decreasing farther inland (their Figure 8). Further, Rutz et al. (2014) determined two corridors of high AR frequency into northern Montana and the Snake River Plain in south-central Idaho.

Studies have also examined different pathways for moisture from the U.S. West Coast into the intermountain west. Rutz et al. (2015) used ERA-Interim data to calculate trajectories starting within ARs as they intersected the U.S. West Coast. These trajectories were then categorized as coastal-decaying, inland-penetrating, or interior-penetrating, depending on how far they traveled while remaining within the AR. They determined that most trajectories made landfall north of ∼40.5°N, although only ∼25% become inland-penetrating, and even fewer become interior-penetrating. Further, about a quarter of the trajectories make landfall between 32.5°N and 40.5°N. These trajectories then split around the Sierra Nevada, with only about 8% of trajectories making landfall south of 32.5°N (Rutz et al., 2015). Swales et al. (2016) used self-organizing maps of IVT to further examine the moisture pathways of ARs. Similar to Rutz et al. (2015), they identified three pathways: northern, central, and southern, with the northern pathway being the most frequent. Further, the southern pathway accounted for 40%–50% of the extreme precipitation events in the southwestern U.S., and the central pathway up to 40% of extreme precipitation events in southern Idaho (Swales et al., 2016). Cann and Friedrich (2020) ran backward HYSPLIT trajectories from the Payette region of Idaho, combined with hourly IVT analyses from the High-Resolution Rapid Refresh model, to determine which moisture pathways contribute to Idaho's mountainous snowfall. They identified the same three trajectories as Rutz et al., 2015 and found that ∼42% of the time, air parcels were blocked and redirected by the Sierra Nevada. Further, the blocked trajectory path retained the highest percentage of IVT (Cann & Friedrich, 2020). These studies use model data and complex methods for tracking trajectories and/or attributing precipitation to ARs. None use observational data and a model designed to track subtropical moisture to quantify the role of subtropical moisture during an AR event over the interior West.

The opportunity to do so follows recent studies that have used the Weather Research and Forecasting model with water vapor tracers (WRF-WVT) to capture AR moisture flux out of the tropics to higher latitudes. First introduced in Miguez-Macho et al. (2013), WRF-WVT allows tracking different moisture sources throughout a model run. Dominguez et al. (2016) used WRF-WVT to quantify the contribution of oceanic evaporation and terrestrial evapotranspiration to precipitation within the North American Monsoon. WRF-WVT was also used in Eiras Barca et al. (2017) to determine the moisture sources for two extreme ARs. Insua-Costa and Miguez-Macho (2018) provide a detailed description of the WRF-WVT code and compare a Pacific AR making landfall on the U.S. West Coast with an Atlantic AR making landfall on the Iberian Peninsula. They found 85% of the moisture in the U.S. West Coast AR was of tropical origin, while 60% of the moisture was tropical in the Iberian Peninsula case. In Hu and Dominguez (2019), WRF-WVT was used to quantify the contribution of tropical Pacific moisture to ARs based on direct contribution, thermodynamic feedbacks, and synoptic-scale dynamic feedbacks. They found that ARs with tropical moisture contributions were associated with stronger pre-cold-frontal low-level jets and stronger warm air advection. Finally, Rauber et al. (2020) used WRF-WVT to evaluate the contribution of tropical moisture to the structure and precipitation of an AR in the southern hemisphere. They found that more than 70% of the precipitation over Australia associated with this AR was tropical in origin, with this percentage decreasing farther south over the Southern Ocean.

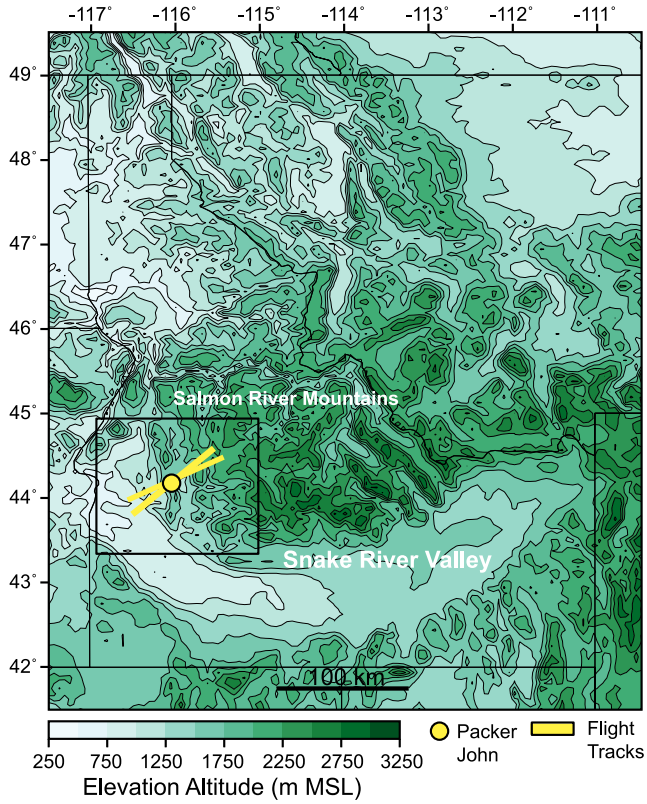

Figure 1. State of Idaho showing the topography of the Salmon River Mountains and the Snake River Valley. The Payette River Basin is on the west side of the Salmon River Mountains. Yellow lines denote the two Wyoming King Air flight tracks used in intensive operation periods 4 and 5. Yellow dot denotes Packer John Mountain. The black square denotes the location of the Seeded and Natural Orographic Wintertime Clouds: The Idaho Experiment campaign.

Wet years on the U.S. West Coast are characterized by a large number of landfalling ARs. In the first two decades of the 21st century, only four wet years occurred on the U.S. West Coast. The year 2017 was one of these four, the second wettest winter in the previous 30 yr (Gershunov et al., 2019; Tessendorf et al., 2019). During 2017, the Seeded and Natural Orographic Wintertime Clouds: The Idaho Experiment (SNOWIE) took place over the Payette River Basin within the Salmon River Mountains of central Idaho between January and March (Figure 1). SNOWIE aimed to examine and quantify the impact of cloud seeding on orographic cloud and precipitation processes (Tessendorf et al., 2019). During SNOWIE, ARs were frequent along the U.S. West Coast, and were followed by heavy snowfall events over the Salmon River Mountains. Several intensive operation periods (IOPs) occurred during or immediately following AR landfall, allowing the opportunity to study the impact of ARs on orographic cloud structure and precipitation. All data from SNOWIE used in this paper are available through the National Center for Atmospheric Research (NCAR, 2022). In this paper, we focus on an AR that impacted precipitation in the Salmon River Mountains for 44 continuous hours and provide a quantitative assessment of the role of subtropical moisture within the AR to the flux of water vapor into the Salmon River Range and on the precipitation across the range.

This research was motivated by questions in the SNOWIE project concerning aerosol source regions, particularly aerosols which can act as ice-nucleating particles or cloud condensation nuclei. During SNOWIE, exceptionally low (typically <40 cm^{-3}) supercooled droplet concentrations were observed during many flights, values much lower than observed in marine cumulus (e.g., Colón-Robles et al., 2006). Although ice-nucleating particle concentrations were not measured in SNOWIE, it was likely that these particles were also in low concentrations. The hypothesized reason for the low concentrations was that air parcels transported over long distances from the subtropics through ARs had been decoupled from surface aerosol sources and subject to aerosol removal processes through precipitation all along their trajectories within the ARs. This motivated the question of where the moisture sources were for precipitating cloud systems over the Idaho Mountains.

To carry out this research, the AR was simulated using WRF-WVT. Distinct from previous studies, here WRF-WVT is configured to isolate the subtropical moisture contribution within the AR to a mountain river basin in the interior of the northwestern U.S. Specifically, subtropical water vapor advected by the AR into the Payette River Basin of Idaho is tagged and tracked in three-dimensional space throughout the run, allowing the contribution of the subtropical moisture to the vertical distribution of water vapor as well as the precipitation to be directly calculated. Additionally, these results are compared to in-situ observations of cloud structure collected by the Wyoming Cloud Radar (WCR) during SNOWIE. The University of Wyoming radar data is available from the University of Wyoming (University of Wyoming 2023).

2. Methodology

WRF version 3.4.1 equipped with water vapor tracers was used in this study. Introduced initially in Miguez-Macho et al. (2013), WRF-WVT tracks moisture originating in, advecting through, or evaporating from a three-dimensional region within the model. Six new variables were created for the traced moisture, allowing for tracing across different hydrometeor species (water vapor, cloud water, rain, ice, snow, and graupel). A complete discussion of WRF-WVT can be found in Insua-Costa and Miguez-Macho (2018). Here, WRF-WVT ran for 105 hr with a time step of 54 s, beginning 3 days and 6 hr before SNOWIE IOP 4 (18–19 January 2017, 18–04 UTC) and ending 3 hr after IOP 5 (19 January 2017 12–19 UTC). Hourly model output files were saved for the run. The domain covered the western United States and eastern Pacific Ocean on a 9 km grid with 32 vertical levels (Figure 2). The large domain was chosen to capture the AR while it strengthened in the Pacific Ocean and made landfall on the U.S. West Coast, and moved into the interior. Water vapor originating in, advecting through,

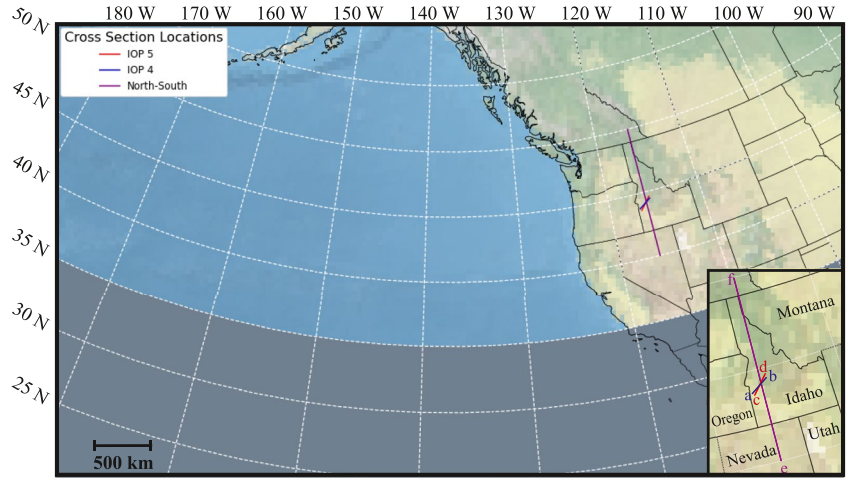

Figure 2. WRF domain with source region for Weather, Research, and Forecasting model with water vapor tracers shaded and cross-section domains indicated. Inset shows the locations of cross-sections in Figures 9–14.

or evaporating from latitudes south of 35°N was tracked. In this paper, we use the term "subtropical" to refer to this moisture, although further back in time, the moisture could have passed through tropical latitudes. The WVTs only track water vapor within the model domain, so to fully capture the moisture field, the domain was extended westward to between 170° and 180°W (Figure 2). Following Insua-Costa and Miguez-Macho (2018), the WRF Single-Moment 6-class (WSM-6) microphysics scheme and Kain-Fritsch convective parameterization were used. Due to the shorter run time compared to Insua-Costa and Miguez-Macho (2018), spectral nudging was not used. For convenience, we will refer to analyses showing IVT and other variables from water vapor originating at all latitudes as WRF and analyses from water vapor originating south of 35°N as WRF-WVT.

AR analyses from NOAA's Automated Atmospheric River Detection Tool (ARDT, NOAA, 2022) were used to determine the time of initiation and the placement of the tracers. The ARDT uses a thresholding technique to detect AR conditions in the Global Forecasting System model (GFS). AR conditions are analyzed every 6 hr, with an archive dating back to 1 October 2016. For an AR to be detected, IVT must be greater than 500 kg $m^{-1}s^{-1}$, with a long axis greater than 1,500 km and a short axis less than 1,000 km. Our determination that this event was an AR was based on criteria set by both Ralph et al. (2019) and the ARDT. The AR was identified in the ARDT database as an AR, and met the Ralph et al. (2019) criteria as a category 3–4 AR based on IVT values at the Oregon/Washington coast of 750 kg $m^{-1}s^{-1}$ < IVT < 1,250 kg $m^{-1}s^{-1}$ over a period of 36 hr. Based on NOAA's ARDT, the choice was made to initialize the model on 15 January 2017 at 12 UTC and track water vapor originating from latitudes south of 35°N (Figure 2). This choice was made because the moisture in the developing AR was still nearly all south of 35°N. Note that there was a separate storm system to the northeast of the developing AR. This storm moved north-northeastward into Canada and never impacted Idaho, so the moisture associated with this storm had no impact on the results shown below. To remain consistent with the ARDT, GFS data was used to drive the WRF-WVT model. The model was initialized with GFS data and used GFS-determined boundary conditions every 3 hr.

During SNOWIE, the University of Wyoming King Air (UWKA) aircraft flew over the Payette River Basin carrying the WCR. The WCR is a 95 GHz, 3 mm wavelength Doppler cloud radar with antennas pointed at zenith and nadir. The WCR measured equivalent reflectivity factor (Z_e) at 30 m resolution along the radar beam and in 4.5–7.5 m increments along the flight track during each flight. At 3 mm wavelength, WCR measurements can be negatively impacted by attenuation, especially in regions of liquid hydrometeors. However, the clouds sampled during SNOWIE mainly were comprised of ice, and no drizzle droplets with diameters greater than 0.5 mm were observed (Majewski & French, 2020). In this study, Z_e measurements from the WCR are used to compare model output to observed cloud structures over the Payette River Basin.

3. Results

Figures 3 and 4 compare IVT calculated using total water vapor from WRF to IVT calculated by the ARDT every 12 hr from 15 January 2017 12 UTC to 19 January 2017 00 UTC. Both domains have been plotted using the ARDT

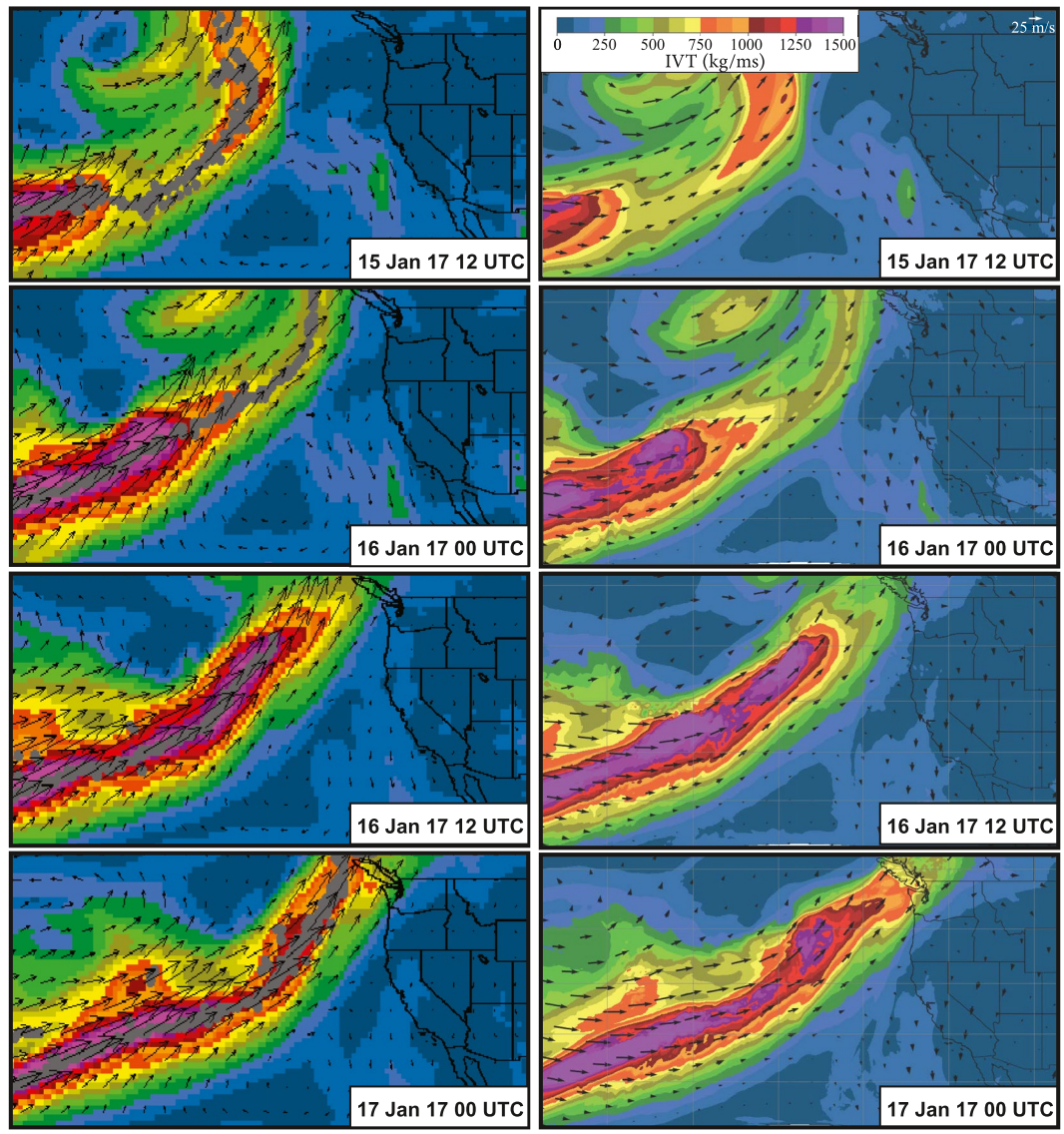

Figure 3. Integrated water vapor transport (IVT) from the ARDT (left) and WRF (right) calculated every 12 hr. Vectors indicate the speed and direction of the wind associated with the IVT (integrated from 100 to 1,000 mb). Gray area on the ARDT plots show the axis of the AR (ARDT figures courtesy of NOAA, 2022).

Mercator projection for ease of comparison. IVT values within the core of this AR reached 1,250 kg $m^{-1}s^{-1}$ for more than 24 hr. With the exception of overestimating IVT values in the core of the AR toward the end of the simulation, WRF replicated the results of the ARDT well (Figures 3 and 4). For example, both models attain a maximum IVT value of 1,500 kg $m^{-1}s^{-1}$ and a northward extent of 50°N at 16 January 2017 12 UTC. Additionally, the AR made landfall at 17 January 2017 00 UTC and began to impact the SNOWIE domain 24 hr later in both the ARDT and WRF simulation.

Figures 5 and 6 compare IVT from WRF to IVT from WRF-WVT. WRF-WVT captured similar values of IVT as WRF within the core of the AR south of the axis of maximum IVT, with more than 90% of the IVT from WRF captured by WRF-WVT. This implies that nearly all of the moisture south of the axis of maximum IVT within the AR's core was sourced from south of 35°N (Figures 5 and 6). Within the core of the AR, where IVT values are the greatest, WRF (Figures 5f–5j and 6f–6j) and WRF-WVT (Figures 5a–5e and 6a–6e) both reach IVT values of 1,500 kg m^{-1} s^{-1}. Additionally, more than 80% of the IVT within the core of the AR is captured by WRF-WVT (Figures 5k–5o and 6k–6o). Toward the southeast boundary of the AR early in the event, low values of IVT in WRF extended farther eastward along the Washington-Oregon coastline than in WRF-WVT, implying that some

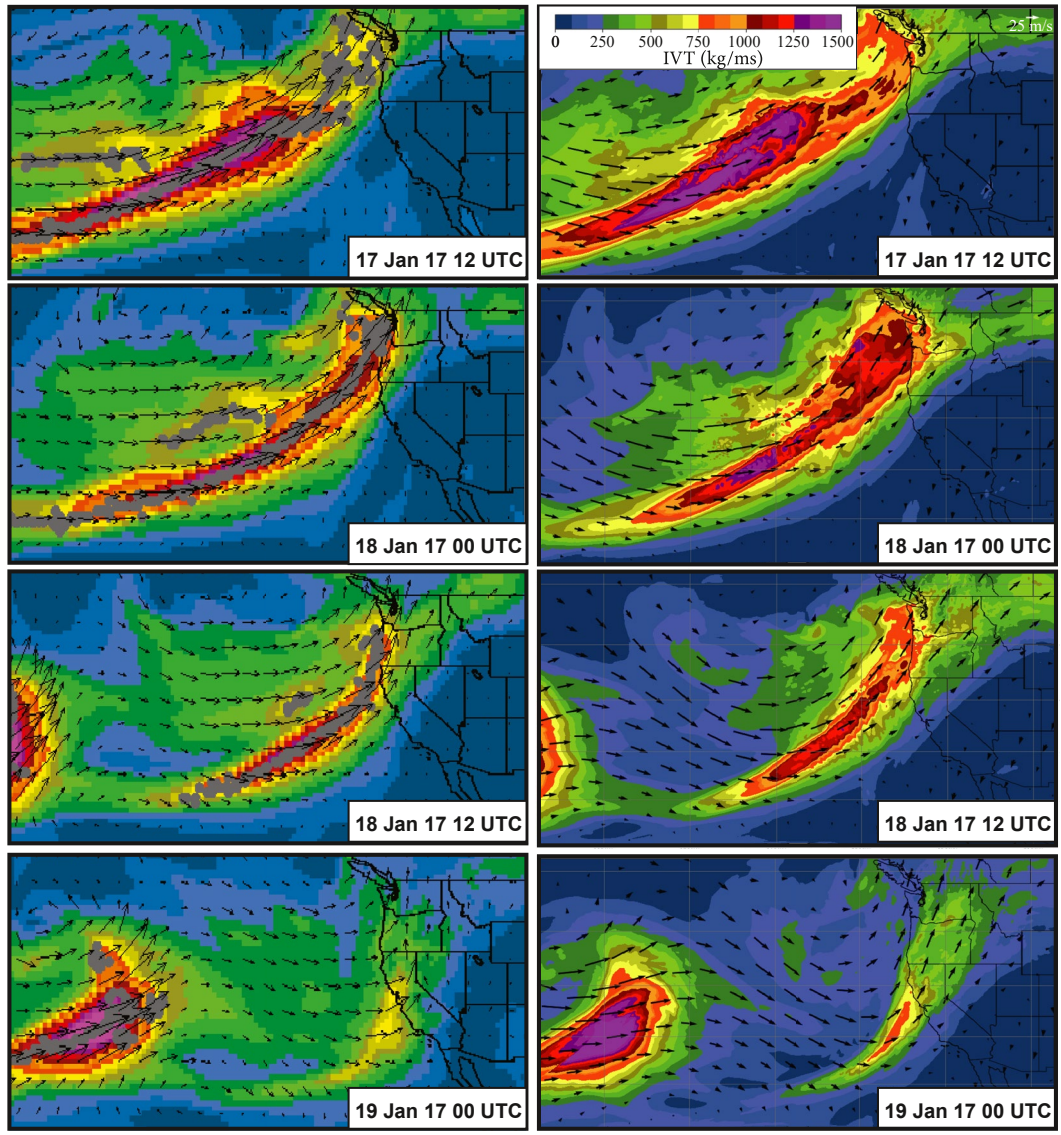

Figure 4. Integrated water vapor transport (IVT) from the ARDT (left) and WRF (right) every 12 hr. Vectors indicate the speed and direction of the wind associated with the IVT (integrated from 100 to 1,000 mb). Gray area on the ARDT plots show the axis of the AR (ARDT figures courtesy of NOAA, 2022).

of the earliest moisture arriving at the west coast sourced from north of 35°N (compare Figures 5c and 5h). Throughout most of the event, a relatively sharp cut-off of moisture appears in WRF-WVT north of the axis of maximum IVT over the Pacific. In contrast, the moisture in WRF extends farther northward, again implying that some of the moisture north of the axis of maximum IVT was drawn from latitudes north of 35°N. Since the axis of maximum IVT remained west of Idaho throughout the simulation, it is unlikely that moisture originating north of 35°N contributed much, if at all, to the precipitation over the Idaho Mountains. Figures 5 and 6 provide confidence that WRF-WVT captured most of the AR moisture advected into central Idaho and that much of the moisture was sourced from the subtropical Pacific.

3.1. Overview of Moisture Flux Over Idaho During SNOWIE IOPs 4 and 5

Figure 7 shows a time series over Packer John Mountain (Figure 1) of relative humidity with respect to ice (RH_i; Figure 7a); WRF water vapor mixing ratio (q) and WRF-WVT water vapor mixing ratio (q_t; Figure 7b); and q and the ratio of q_t to q (Figure 7c). The RH_i time series (Figure 7a) shows the cloud field arriving at Packer John at

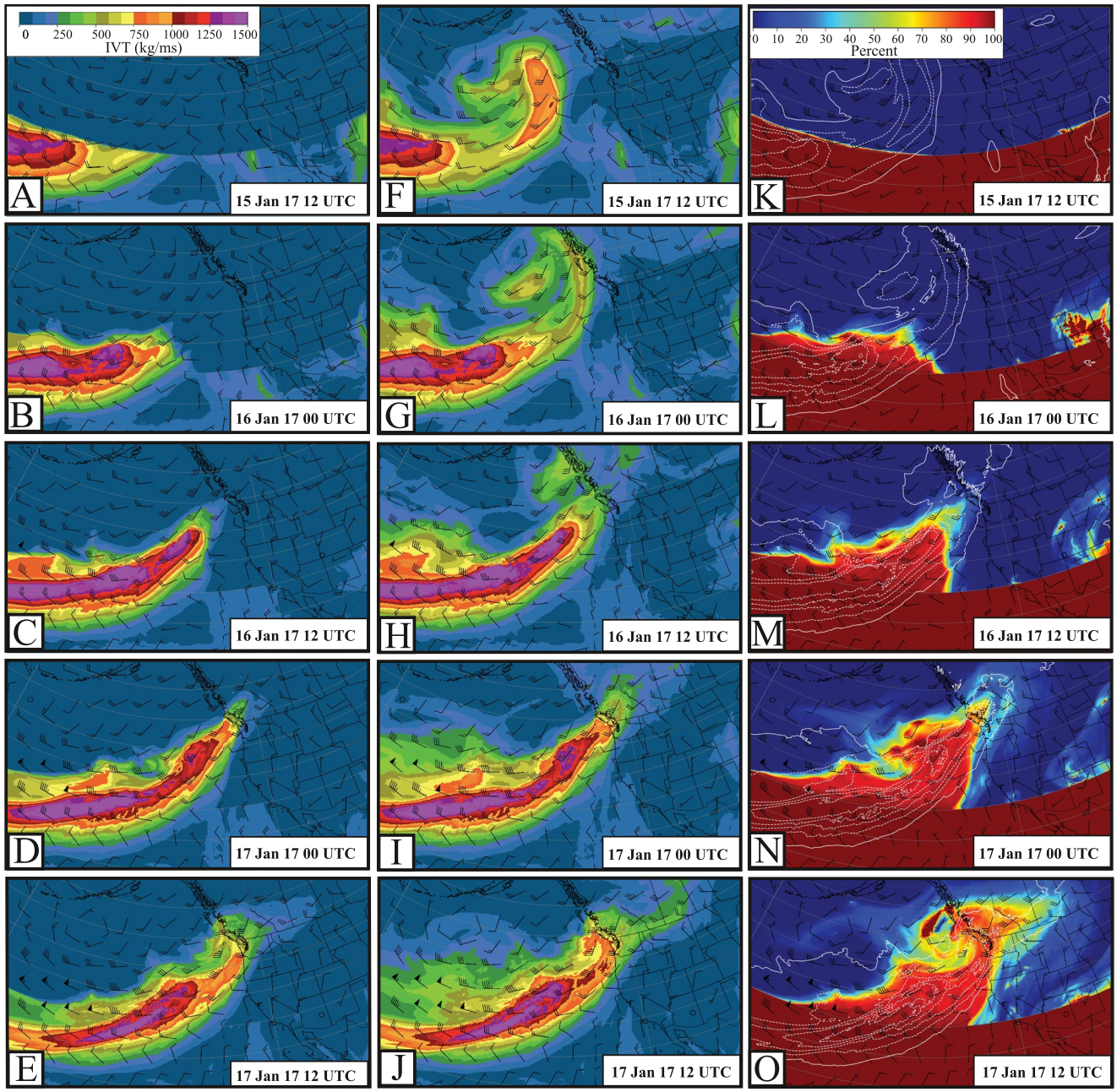

Figure 5. Weather, Research, and Forecasting model with water vapor tracers (WRF-WVT) integrated water vapor transport (IVT; left), WRF IVT (center), and ratio of WRF-WVT IVT to WRF IVT (%, right) at the same times as Figure 3. Winds are averaged over 1,000–100 hPa in m s^{-1} (consistent with the ARDT) with a long barb = 10 m s^{-1}.

18 January 2017 12 UTC. However, subtropical moisture starts arriving at Packer John ahead of the cloud, with values of q_t exceeding 2 g kg^{-1} by 18 January 2017 00 UTC (Figure 7b). Furthermore, the subtropical moisture initially arrives in the mid-troposphere, above 600 hPa, before appearing closer to the surface. The greatest influx of subtropical moisture coincides with the cloud field impacting Packer John after 18 January 2017 12 UTC. At this time, $q_t > 3.5$ g kg^{-1} in the lower troposphere. Finally, the contribution of q_t to q is high. Above 700 mb and before 19 January 2017 12 UTC, q_t accounts for more than 80% of q (Figure 7c).

A cloud is present over Packer John throughout IOP 4 (Figure 7a). More subtropical moisture is present overall, with values of $q_t > 3.5$ g kg^{-1} near the surface, and the contribution of q_t to q is greater than 70% throughout this cloud (Figure 7b). During IOP 5, the cloud is still present, however a region of dry air appears toward the end

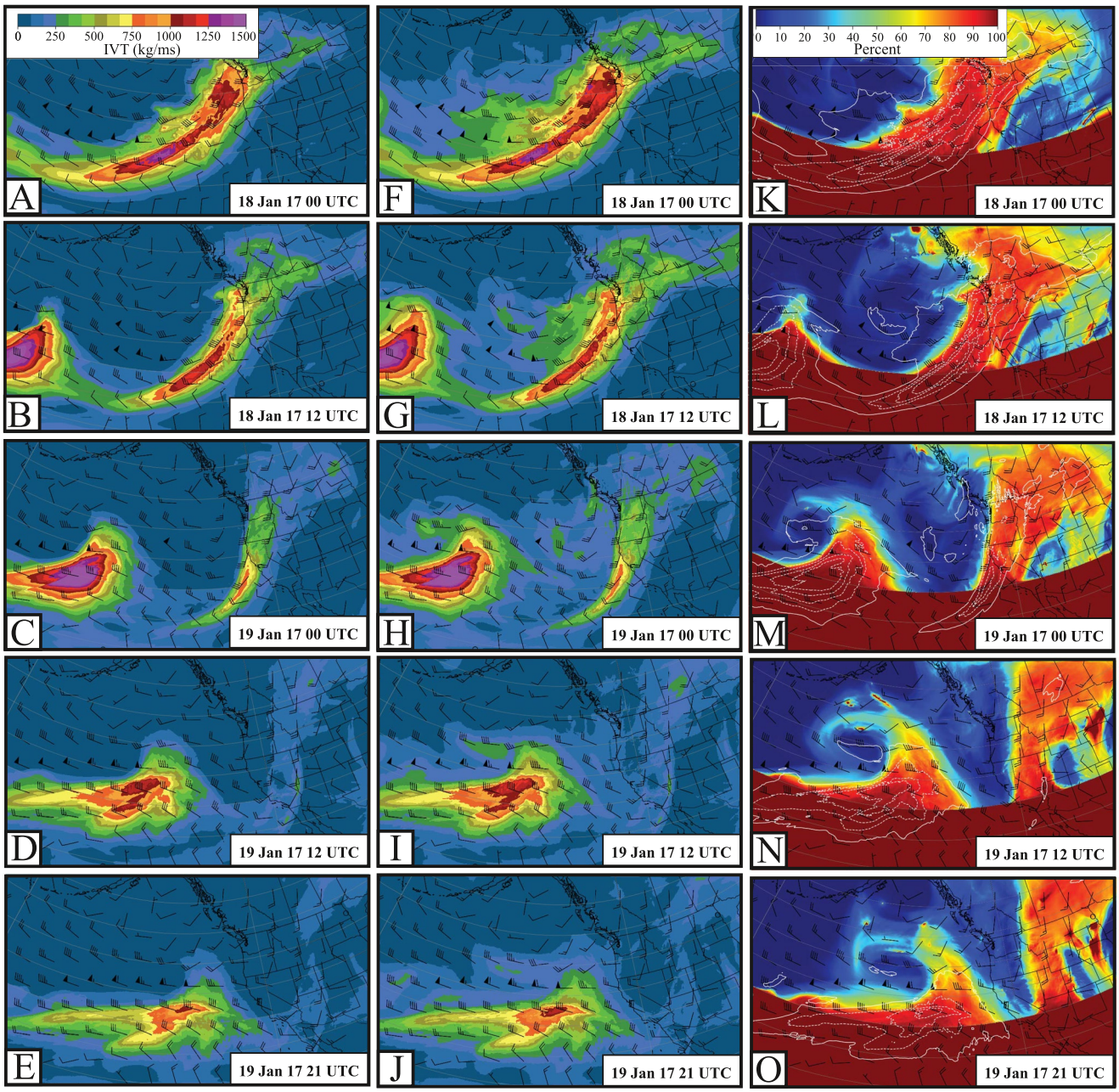

Figure 6. Weather, Research, and Forecasting model with water vapor tracers (WRF-WVT) integrated water vapor transport (IVT; left), WRF IVT (center), and ratio of WRF-WVT IVT to WRF IVT (%, right) at the same times as Figure 4. Winds are averaged over 1,000–100 hPa in m s^{-1} (consistent with the ARDT) with a long barb = 10 m s^{-1}.

(Figure 7a). Before this dry air appears, the contribution of q_t to q is greater than 70% above 700 hPa, and greater than 60% below 700 hPa. After the dry air arrives, the contribution of q_t tapers off to 60% everywhere (Figure 7c). Less subtropical moisture is present during IOP 5, with $q_t < 3$ g kg^{-1} everywhere.

3.2. IOP 4

As shown in Figures 5 and 6, the AR developed during the 3 days prior to SNOWIE IOP 4. The AR first made landfall on the west coast at approximately 16 January 2017 12 UTC and began impacting the central Idaho Mountains at 18 January 2017 00 UTC. IOP 4 took place between 18 January 2017 18 UTC and 19 January 2017

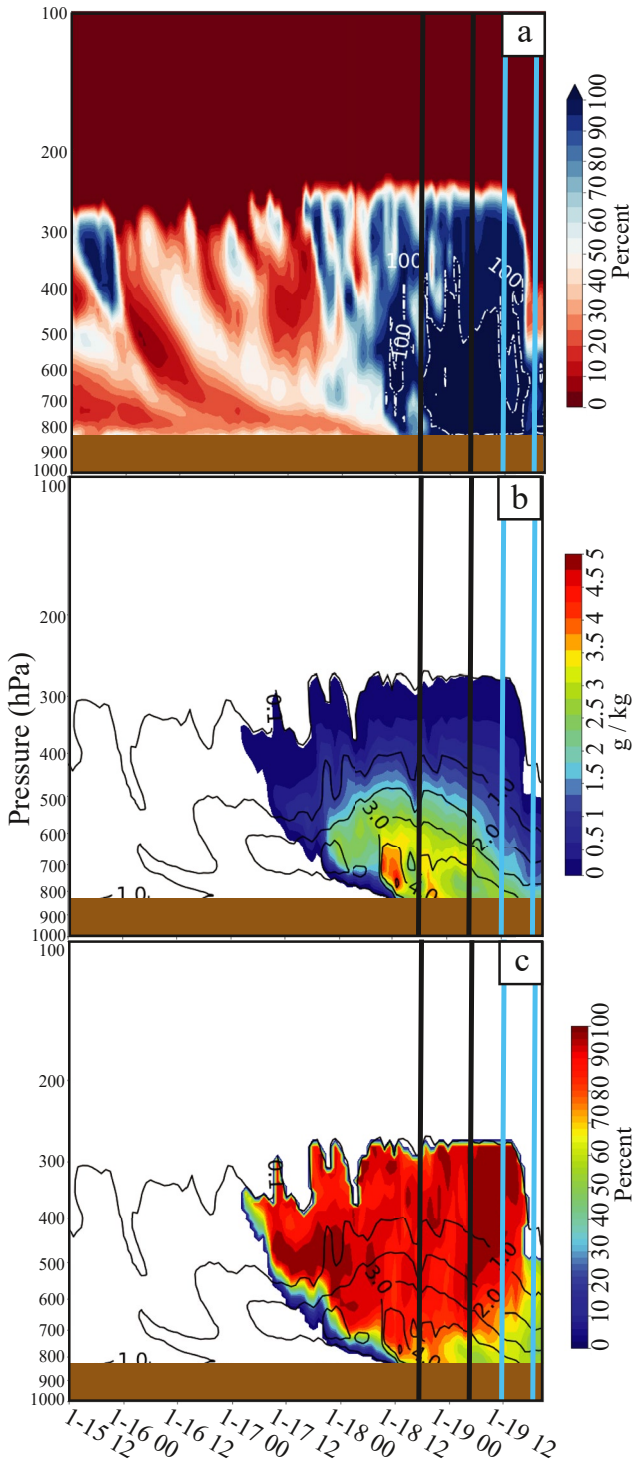

Figure 7. Time series of (a) RH_i, inside of dashed white line RH_i >100%, (b) contours (q, g kg^{-1}) and colors (q_t), (c) contours (q, g kg^{-1}) and colors (q_t/q *100%) over Packer John Mountain. Vertical black lines indicate IOP 4; blue lines indicate IOP 5. The outer contour is 0.1 g kg^{-1}.

04 UTC. The UWKA operated for 3 hr, from 18 January 2017 20 UTC to 23 UTC, during which the cloud system was sampled along a southwest to northeast flight track over the western slopes of the Salmon River Mountains. During IOP 4, the AR impacted the SNOWIE domain (Figures 8a–8c), while during IOP 5, the remnants of the AR remained over the SNOWIE domain but were rapidly moving eastward (Figures 8d–8f). As shown in Figures 5–8, the AR impacted the SNOWIE domain for the duration of the IOP, with WRF IVT values exceeding 250 kg m^{-1}s^{-1} over Idaho throughout the IOP and WRF-WVT IVT values ranging from 250 kg m^{-1}s^{-1} at the beginning of the IOP to 166 kg m^{-1}s^{-1} at the end. This indicates that as the AR moved over the Idaho Mountains, much but not all of the moisture was sourced from latitudes south of 35°N.

Figure 9 compares vertical cross-sections of WCR equivalent reflectivity factor, Z_e, (Figures 9a and 9b) to cross-sections of RH_i from WRF (Figures 9c and 9d). Both cross-sections are taken along the Wyoming King-Air's flight track during IOP 4 (see Figure 2), with the WRF RH_i fields calculated from the closest hour to the WCR's operation. At 18 January 2017 21 UTC, the WCR sampled a shallow cloud layer, with cloud echo tops near 6 km on the western end and 5 km on the eastern end of the cross-section over the Salmon River Mountains (Figure 9a). The Z_e within the cloud layer was generally less than 0 dBZ, with fall streaks marginally exceeding 0 dBZ. WRF calculated RH_i values near or exceeding 100% throughout the cloud depth, with most of the layer supersaturated with respect to ice. Because of the difference in resolution between the WCR and WRF, fine-scale details of the cloud structure were not simulated, however, the overall cloud depth and level of ice saturation corresponded well with each other. Figure 9b shows a deepening of the cloud layer later during IOP 4. By 18 January 2017 23 UTC, the WCR observed clouds extending to 10 km above MSL, with Z_e values exceeding 10 dBZ below 6 km. At the same time, WRF calculated RH_i values of 100% up to 8 km, with a supersaturated region (with respect to ice) between 2 and 6 km.

Figures 10a and 10b each show q (contours) and q_t (color fill) in g kg^{-1} at 18 January 2017 21 UTC and 23 UTC, respectively. Figures 10c and 10d each show q (contours) and the contribution of q_t to q as a percentage (color fill) at the same times. All fields in Figure 10 are calculated along the UWKA's flight track at the nearest hour to the WCR fields in Figures 9a and 9b. At 18 January 2017 21 UTC, most of the water vapor is contained in the lowest 6 km of the atmosphere, with q values ranging from over 5 g kg^{-1} at the surface to 1 g kg^{-1} at 6.5 km (Figure 10a). This is consistent with the cloud top height detected by both the WCR and calculated in the RH_i field. Furthermore, as shown in Figure 10c, more than 70% of the moisture in the lower troposphere originated south of 35°N, with the percentage increasing to >90% above 4 km. At 18 January 2017 23 UTC, more water vapor was now present at higher altitudes, with the 1 g kg^{-1} q contour extending to about 7 km (Figure 10b). This is consistent with the WCR observation of a deepening cloud layer during IOP 4. Additionally, below 2 km, some moisture of non-tropical origin is present in the lower troposphere. HYSPLIT back trajectories suggest that some of this midlatitude low-level moisture originated 48 hr earlier in interior valleys of the western U.S. (not shown). However, above 2 km, more than 80% of the moisture within the cloud is WRF-WVT moisture, with that percentage approaching 100% with increasing altitude (Figure 10d).

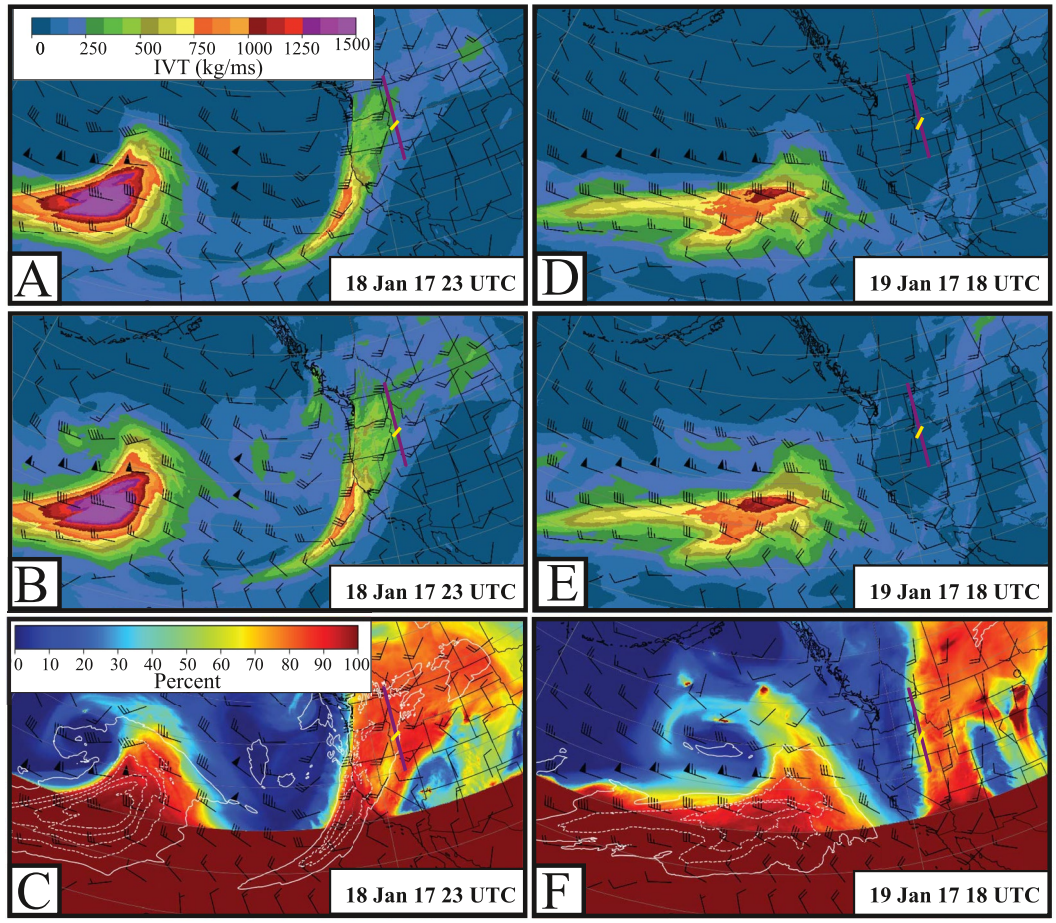

Figure 8. Weather, Research, and Forecasting model with water vapor tracers (WRF-WVT) integrated water vapor transport (IVT; top), WRF IVT (center), and ratio of WRF-WVT IVT to WRF IVT (%, bottom) at the end of IOP 4 (a–c) and the end of IOP 5(d–f). Locations of cross-sections indicated in yellow and purple. Winds are averaged over 1,000–100 hPa in m s^{-1} with a long barb = 10 m s^{-1}.

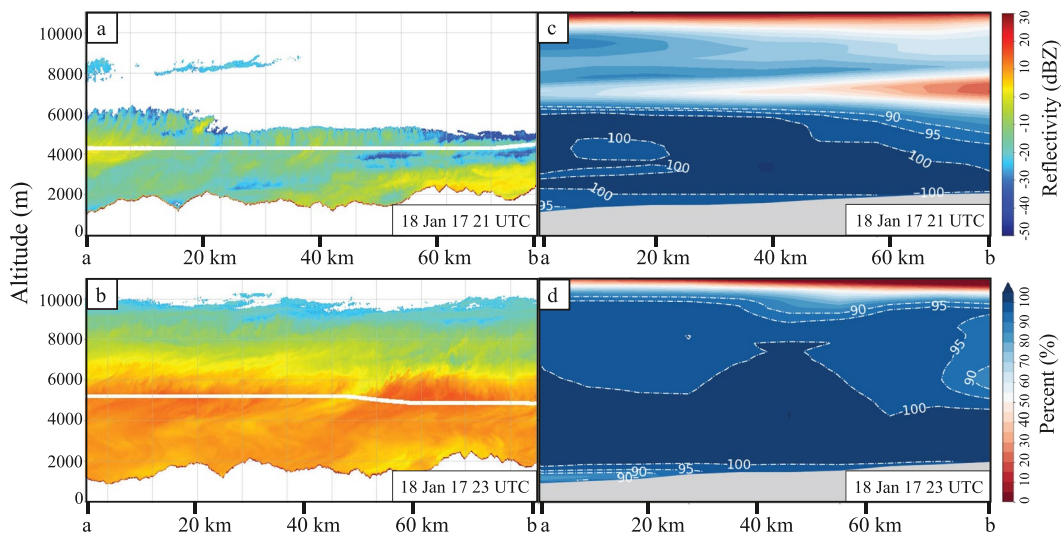

Figure 9. Cross-sections along (a–b) in Figure 2. (a, b) WCR Z_e and (c, d) WRF RH_i (color fill + white contours for RH_i >90).

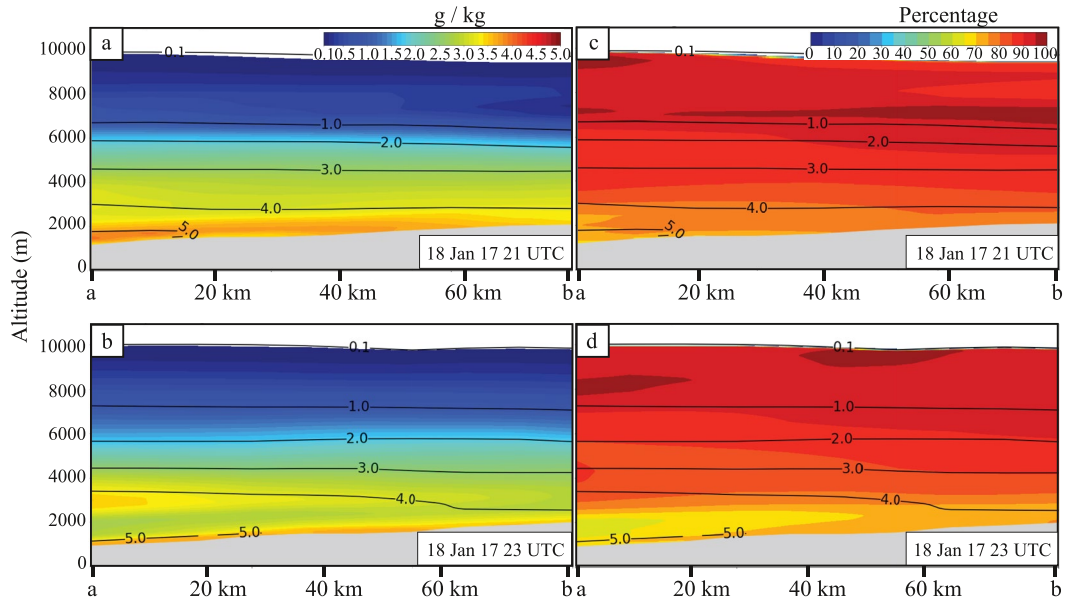

Figure 10. Cross-sections along (a–b) in Figure 2. (a, b) WRF q (contours) and Weather, Research, and Forecasting model with water vapor tracers (WRF-WVT) q_t (color-fill), (c, d) WRF q (contours) and ratio of WRF-WVT q_t to WRF q (q_t/q *100%) (color-fill).

Figure 11 shows the same variables as Figures 9c, 9d, and 10 along a north-south cross section at 116°W longitude (see Figure 2) that passes over the Salmon River Mountains. In the RH_i field (Figure 11a), columns of supersaturation (with respect to ice) mark regions of updrafts on the upwind sides of ridges. The semi-regular spacing of these columns demonstrates the orography's effect on cloud structure. Figure 11b, with contours of q and color fill of q_t, shows that moisture is present up to 10 km, with most of the moisture contained in the lowest 6 km. This is consistent with the RH_i and WCR fields analyzed in Figure 9. Figure 11c shows q (contoured) and the contribution of q_t to q (color fill), as in Figures 10c and 10d. Above 3 km, more than 80% of the moisture originated from latitudes south of 35°N along the entire cross-section. In the lower troposphere, this percentage drops to 60% on the northern side of the domain and to about 5% on the southern side. We speculate that this decrease is due to removal of moisture through precipitation as the airstream crossed the Sierra Nevada and Cascade ranges.

3.3. IOP 5

During IOP 5, which occurred between 19 January 2017, 12 UTC and 18 UTC, remnants of the AR were rapidly moving eastward over the SNOWIE domain. At 19 January 2017 12 UTC, both WRF IVT and WRF-WVT IVT values were less than 167 kg m^{-1} s^{-1}, and this value continued to fall throughout the IOP. The WCR operated for 3 hr, from 19 January 2017 15:30 UTC to 18:30 UTC, sampling clouds along a southwest to northeast flight track (see Figure 2).

Figure 12 shows WCR Z_e (Figures 12a and 12b) compared to WRF RH_i (Figures 12c and 12d) at 19 January 2017 16 UTC and 18 UTC. Both WRF cross-sections are calculated along the UWKA's flight track at the closest hour to the WCR's operation. At 19 January 2017 16 UTC, the WCR sampled a deep cloud on the northeastern end of the flight track and two-layered clouds on the southwestern end (Figure 12a). A cloud top height of about 9 km was detected across the flight track, with a region of dry air between 4 and 6 km propagating from the southwest. This region of dry air caused the previously deep cloud to split. Z_e values throughout this cloud were generally between −20 and 0 dBZ, with fall streaks of 10 dBZ measured. WRF-calculated RH_i values were near 100% throughout the depth of the cloud, with a layer of supersaturation (with respect to ice) below 4 km (Figure 12c). On the northeastern side of the cross-section, RH_i values greater than 90% were calculated to a height of 9 km, while on the southwestern side, this height decreased to 4 km. Additionally, the RH_i field captured the dry layer, with RH_i values dropping below 80% between about 4 and 7 km on the southwestern side of the cross-section. At 19 January 2017 18 UTC, the WCR sampled two distinct clouds (Figure 12b). The lower cloud reached a cloud top height of 4 km, with Z_e approaching 10 dBZ in regions of precipitation. The upper cloud was detected between 6 and 8 km, with Z_e

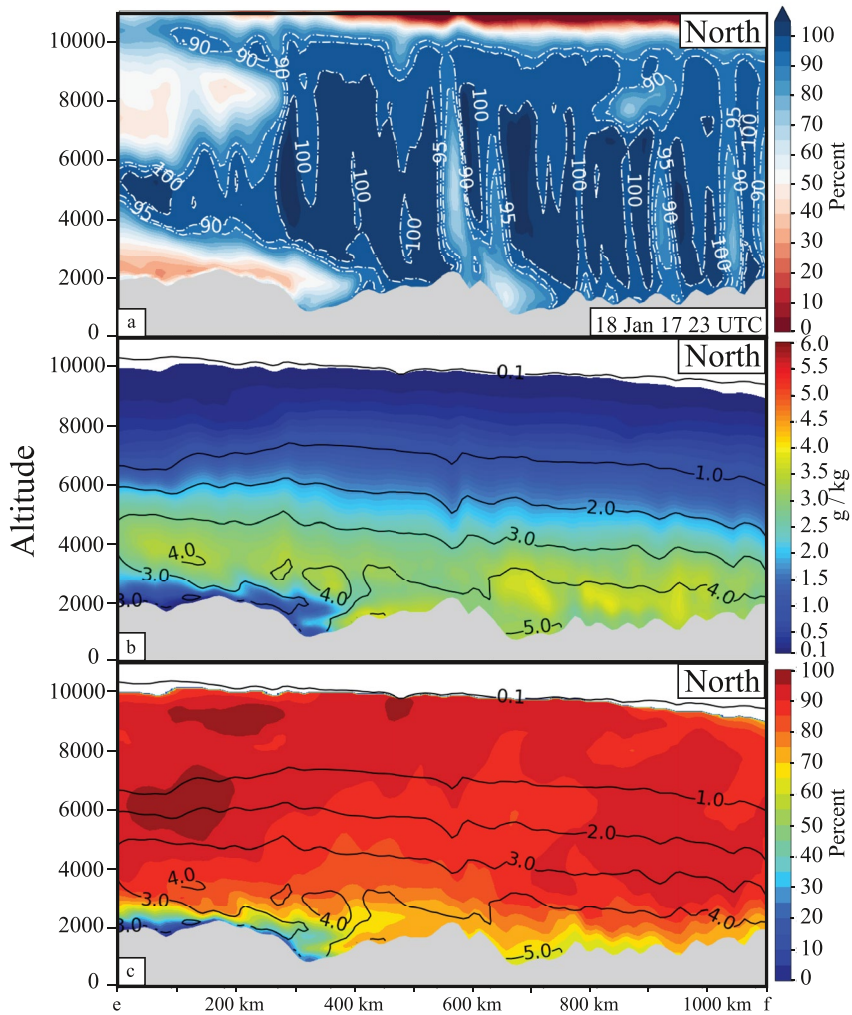

Figure 11. Cross-sections along (e–f) in Figure 2. (a) WRF RH_i (color fill + white contours for RH_i >90%), (b) WRF q (contours) and WRF-WVT q_t (color-fill), (c) WRF q (contours) and ratio of WRF-WVT q_t to WRF q (q_t/q *100%) (color-fill).

less than 0 dBZ throughout the cloud. Between the two clouds, from 4 to 6 km, no cloud particles were sampled. At the same time, WRF-calculated RH_i values were near or exceeded 100% up to a height of 4 km (Figure 12d). The dry layer shown in Figure 12c rapidly moved eastward, eliminating the upper cloud layer entirely.

Figures 13a–13d show the same variables during IOP 5 as Figures 10a–10d, again along the UWKA's flight track. At 19 January 2017 16 UTC, most of the water vapor is contained in the lower troposphere, with q values falling below 1 g kg^{-1} above 4 km (Figure 13a). Additionally, the q_t field corresponds to the RH_i field (Figure 12c), with no moisture present above 9 km on the northeastern side of the cross-section, and a dry air intrusion at 6 km on the southwestern side. Figure 13c shows the contribution of q_t to q at 19 January 2017 16 UTC. Above about 6 km, WRF-WVT moisture contributes to more than 85% of the moisture present across the domain, with this percentage increasing to 100% with increasing altitude. Below 6 km, the contribution of WRF-WVT moisture falls below 85% and approaches 50% just above the ground. At 19 January 2017 18 UTC, the moisture above 6 km has been reduced greatly, with only a small region of $q > 0.1$ g kg^{-1} on the northeastern side of the domain (Figure 13b). Additionally, the dry layer at 6 km is now present along the entire flight track. Figure 13d shows that most of the water vapor present in the upper troposphere is of subtropical origin, with percentage values near 95%. In the lower troposphere, this value decreases to about 70% at 5 km, 60% at 4 km, and continues to decline near the surface.

Figure 14 shows a north-south cross-section along the 116°W longitude at 19 January 2017 18 UTC (see Figure 2). In the RH_i field (Figure 14a), columns of supersaturation again indicate the location of updrafts on the windward

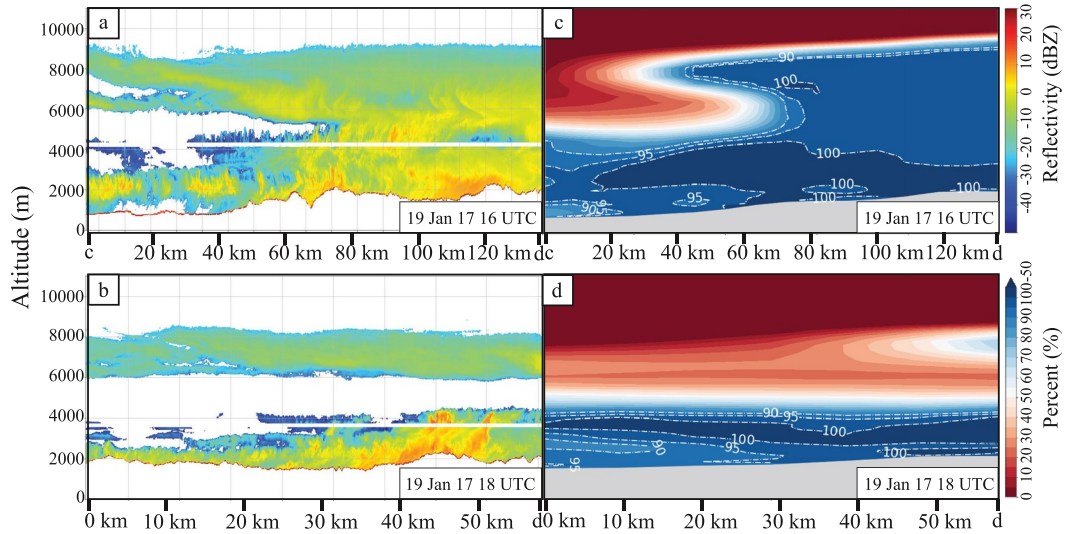

Figure 12. Cross-sections along (c–d) in Figure 2. (a, b) WCR Z_e and (c, d) WRF RH_i (color fill + white contours for RH_i >90%).

side of the mountains and demonstrate the effect of orography on cloud structure (Zaremba et al., 2022). These columns are less apparent than they were in IOP 4; however, they were still present at a semi-regular spacing on the upwind side of ridges. Additionally, dry air intrusions can be seen in the RH_i field, with two regions of RH_i less than 60% extending from 10 km to the surface. The first occurs on the southern side of the domain, and the second on the northern side.

Figure 14b shows q (contoured) and q_t (color-fill). Most of the water vapor throughout the cross-section is located in the lowest 4 km of the troposphere, and all of it is located in the lowest 6 km of the troposphere. Additionally,

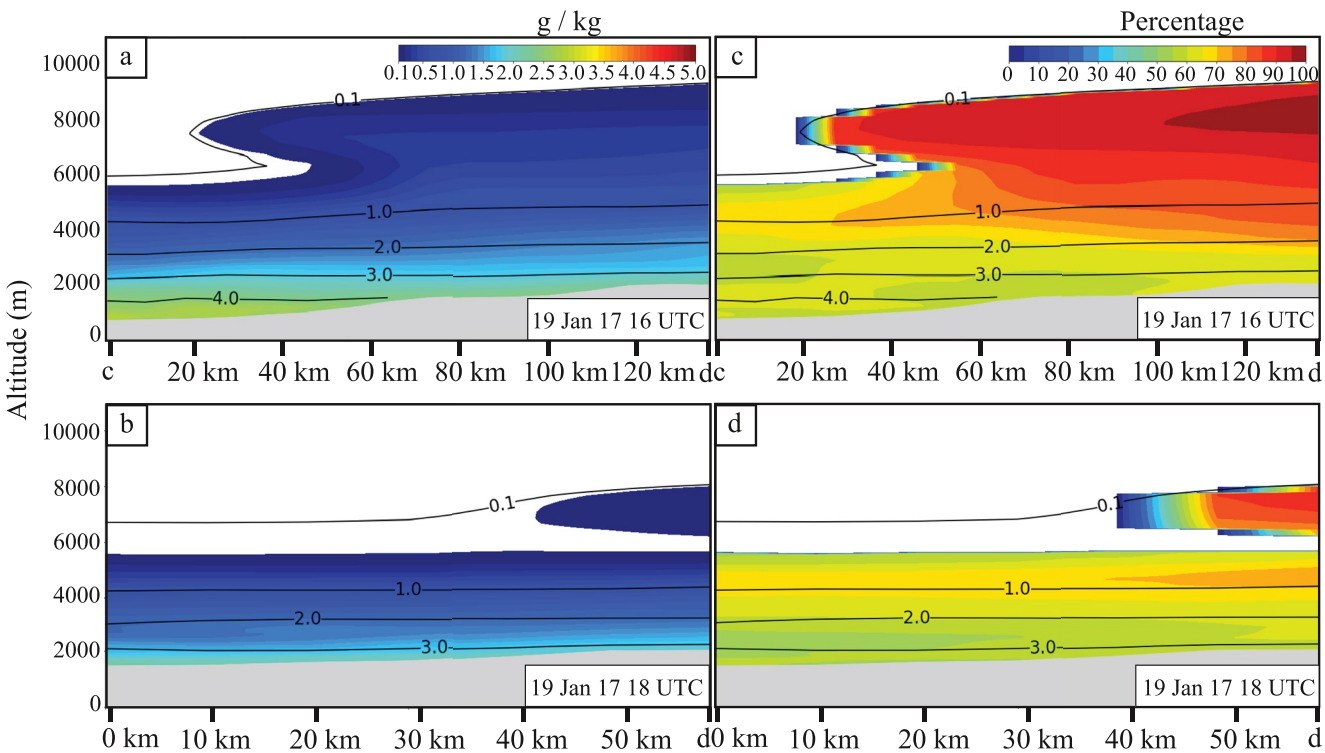

Figure 13. Cross-sections along (c–d) in Figure 2. (a, b) WRF q (contours) and Weather, Research, and Forecasting model with water vapor tracers (WRF-WVT) q_t (color-fill), (c, d) WRF q (contours) and ratio of WRF-WVT q_t to WRF q (q_t/q *100%) (color-fill).

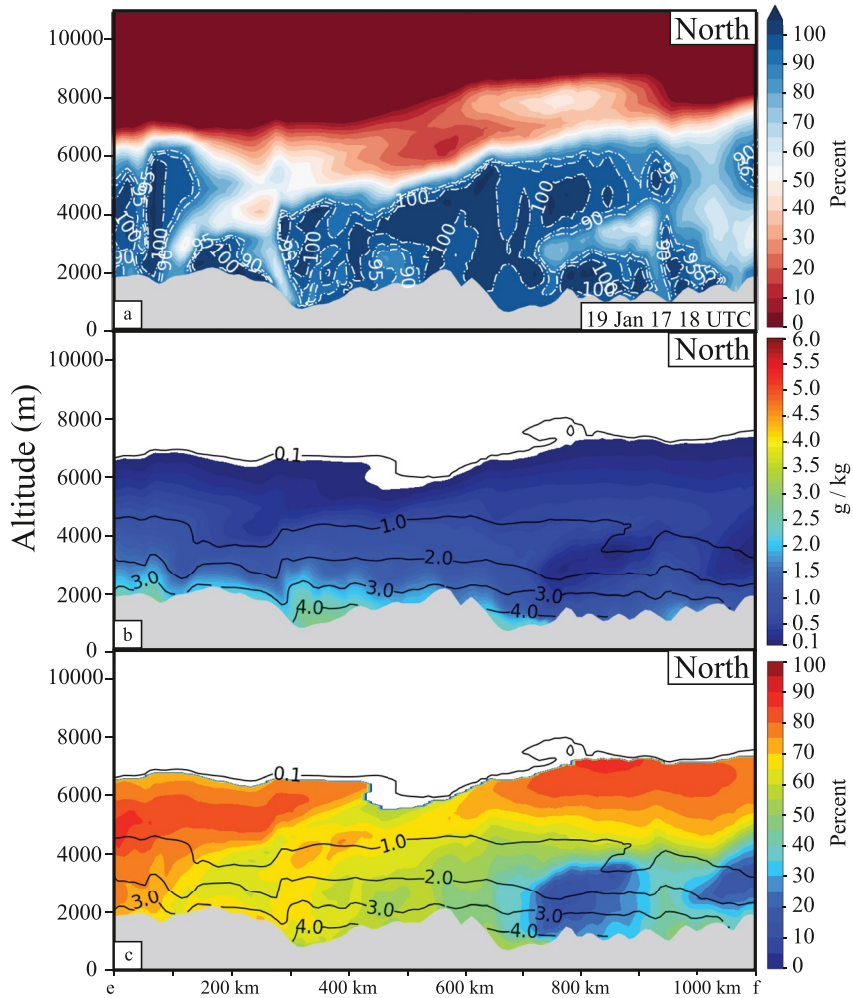

Figure 14. Cross-sections along (e–f) in Figure 2. (a) WRF RH_i (color fill + white contours for RH_i >90%), (b) WRF q (contours) and Weather, Research, and Forecasting model with water vapor tracers (WRF-WVT) q_t (color-fill), (c) WRF q (contours) and ratio of WRF-WVT q_t to WRF q (q_t/q *100%) (color-fill).

the regions of dry air identified in Figure 14a are also present in the q field, indicated by the sudden dips in q-contours. The highest q_t values are found near the surface, with a maximum of ~2.5 g kg^{-1} on the southern side of the cross-section. Above 2 km, q_t values remain below 2 g kg^{-1}. The contribution of q_t to q (Figure 14c) is greatest in the upper troposphere. The lower percentage of q_t to q in the lower troposphere may be due to removal of moisture through precipitation as the airstream crossed the Sierra Nevada and Cascade ranges. On the southern edge of the cross-section, WRF-WVT moisture contributes to 70% of the total moisture near the surface, and this percentage increases to 90% at a height of 5 km. On the northern edge, WRF-WVT moisture contributes to more than 80% of the moisture above 5 km, decreasing to 0% near the surface. There is also a meridional gradient in low-level WRF-WVT moisture contribution across the cross-section, with low-level percentages decreasing from 70% to the south to near 0% to the north. The remnant low-level moisture appearing on the northern side of Figure 14 must have originated from the northern reaches of the AR.

3.4. Precipitation

Figure 15 shows the net precipitation in mm and WRF-WVT precipitation in percent over Idaho during IOP 4 (Figures 15a and 15b), IOP 5 (Figures 15c and 15d), and from the beginning of IOP 4 to the end of IOP 5 (Figures 15e and 15f). A minimum threshold value of 0.2 mm was applied to the figures. During IOP 4, under 10 mm of precipitation fell in the lower elevations and 10–50 mm at higher elevations, with two local peaks of

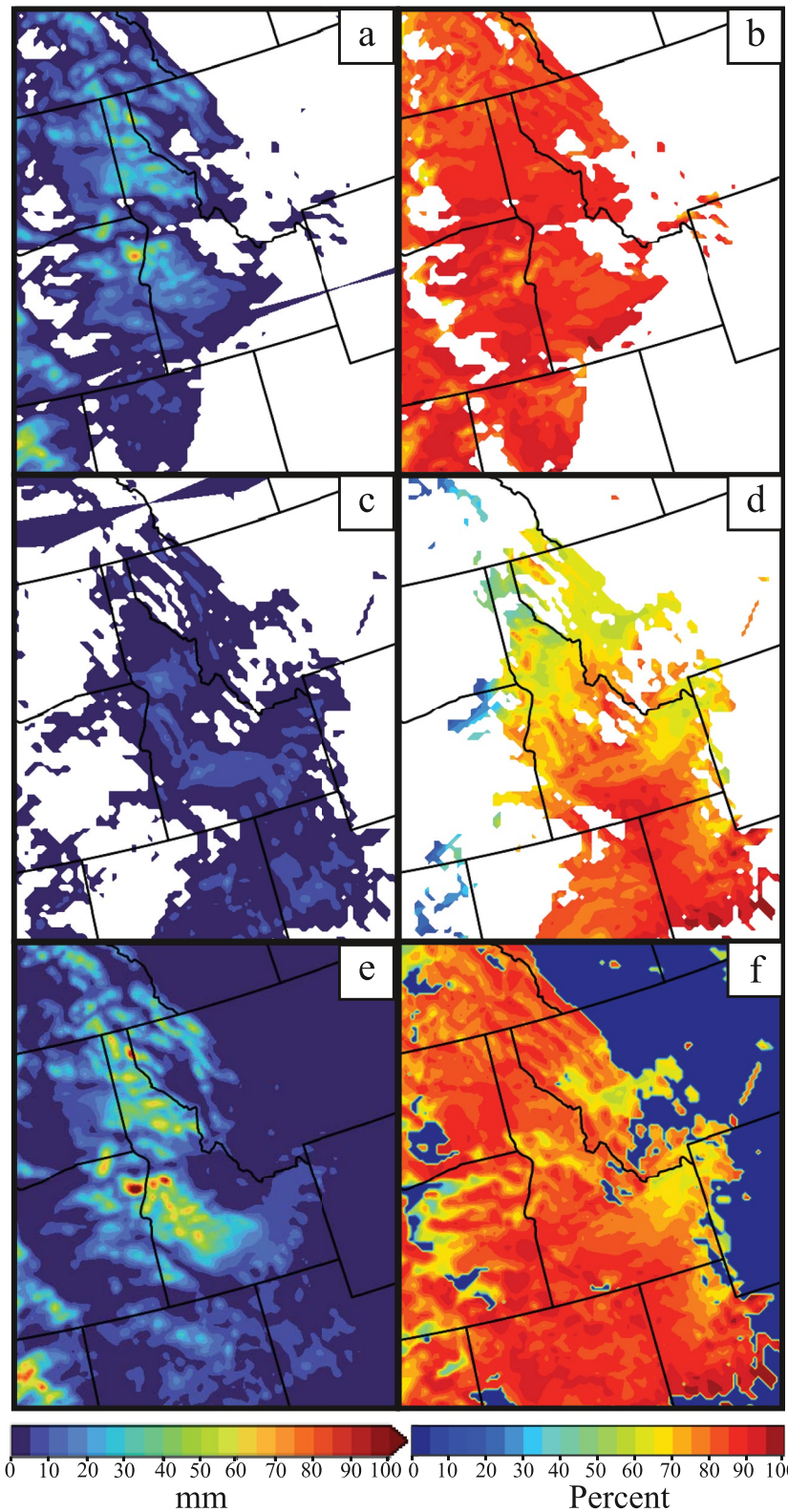

Figure 15. Accumulated precipitation during (a) IOP 4 (c) IOP 5 (e) beginning of IOP 4 to end of IOP 5 and percentage of precipitation from Weather Research and Forecasting model with water vapor tracers during (b) IOP 4 (d) IOP 5 (f) beginning of IOP 4 to end of IOP 5.

even higher amounts. WRF-WVT precipitation contributed to over 80% of the precipitation during IOP 4, with the percentage approaching 100% in several regions (Figure 15b). The simulation results imply that most of the precipitation that fell during IOP 4 resulted from subtropical Pacific moisture.

During IOP 5 (Figures 15c and 15d), less precipitation fell overall, and more of that precipitation came from the part of the AR that originated north of 35°N. Under 6 mm of precipitation fell in the lower elevations and under 15 mm at higher elevations, with local peaks up to 21 mm. Much of this precipitation was still attributed to WRF-WVT moisture. Across Idaho, WRF-WVT water vapor varied in contribution to the total IOP 5 precipitation, ranging from 35% to 60% in the north to >90% in the south. The gradient in WRF-WVT contribution was likely due to the AR's southwest to northeast orientation as it penetrated inland.

Finally, Figures 15e and 15f show the net precipitation during and between both SNOWIE IOPs. Up to 140 mm of precipitation fell at high elevations, while under 40 mm of precipitation fell at low elevations. Most of this precipitation was attributable to WRF-WVT moisture, with the contribution of WRF-WVT moisture greater than 60% everywhere. This percentage increases to 100% at low elevations and at southern latitudes. This percentage decreases toward the east, indicating that the AR subtropical moisture contributed less to total precipitation as the AR remnants moved farther inland.

4. Discussion

In the case studies above, the contribution of subtropical moisture to the total moisture flux was greatest (>80%) at higher altitudes, and less (60%–70%) at lower altitudes (Figures 10, 11, 13, and 14). Nearly all of the non-subtropical moisture must have sourced from over the Pacific Ocean at latitudes north of 35°N, transported into Idaho primarily at low altitudes, and been drawn into the overall AR moisture stream. Because the storm produced rain and snow over the mountains and valleys of the Pacific Northwest, it is also possible that a very small percentage of the moisture arriving in Idaho may have resulted from evaporated precipitation. This moisture would be tagged as midlatitude moisture, even though it may have originally sourced from the subtropics. Since this surface-evaporated moisture was not tagged, it was not possible to estimate this contribution to the overall moisture flux.

Throughout this event, more than 60% of the precipitation across Idaho was attributed to subtropical moisture transported into Idaho by the AR. This percentage is higher than the values found by Dettinger et al. (2011), Rutz and Steenburgh (2012), and Rutz et al. (2014), all of which attributed less than 40% of the precipitation across Idaho to ARs, although they specifically looked at AR-related precipitation and did not discriminate between subtropical and midlatitude moisture sources. Notably, Rutz has offered that he believes the fraction of precipitation attributable to ARs across much of the Interior West is actually higher than his studies show, due to limitations in the methodology of relating AR spatial extent over complex terrain to precipitation (personal correspondence). In addition, these previous studies focused on the impact of ARs on seasonal precipitation across Idaho, which may account for some of the differences. This study shows that subtropical moisture within ARs can significantly contribute to Idaho's precipitation on an individual case basis, even though ARs may contribute less to Idaho's annual precipitation seasonally.

The results presented here agree with those presented in Eiras Barca et al. (2017) in their Figure 7b for Idaho. Eiras Barca et al. (2017) used WRF-WVT to track tropical water vapor in two ARs. In the Pacific AR case, although their analysis focused on coastal mountains, their Figure 7b suggests that about 60% of the precipitation in Idaho could be attributed to subtropical moisture within their AR, with some areas approaching 90%. Additionally, they attributed 70%–90% of the precipitation along the U.S. West Coast to subtropical moisture within their AR.

5. Conclusions

The SNOWIE campaign took place in 2017 over the Payette River Basin within the Salmon River Mountains of central Idaho between January and March. During SNOWIE, ARs were frequent along the U.S. West Coast and influenced the snowfall over Idaho's Salmon River Mountains. In this paper, we quantified the impact of an AR on the flux of moisture across the Salmon River Mountains and precipitation within the mountains. The structure of the clouds was also compared to data collected by the WCR during two SNOWIE IOPs.

WRF-WVT was configured to isolate the contribution of moisture from south of 35°N to the AR moisture flux and precipitation over the Idaho Mountains. Specifically, water vapor advected from south of 35°N by the AR into the Payette River Basin of Idaho was tagged and tracked in three-dimensional space throughout the run. This allowed the contribution of the subtropical moisture to the vertical distribution of water vapor as well as the precipitation to be directly calculated.

Overall, this study found that:

- More than 70% of the moisture flux in the troposphere across the mountains during IOP 4 was attributable to the subtropical moisture advected by the AR
- More than 80% of the precipitation over Idaho during IOP 4 was attributable to the subtropical moisture within the AR
- Nearly all moisture flux in the upper troposphere (above 6 km) during IOP 5 was attributable to subtropical moisture, even post-deep cloud passage
- About 50% of moisture in lower troposphere (below 6 km) was attributable to subtropical moisture during IOP 5
- The subtropical moisture contribution to IOP 5 precipitation ranged from 35% in northern Idaho to more than 90% in southern Idaho
- Across both IOPs, more than 60% of precipitation in Idaho was attributable to subtropical moisture advected within the AR, with this percentage increasing toward the south across the state.

This study demonstrated the potential of using the water vapor tracing tool within WRF to better understand the impact of ARs on the interior mountains of the intermountain western U.S. Future investigations will focus on the seasonal impact of ARs using the tracing technique.

Data Availability Statement

All data presented here are publicly available through the SNOWIE data archive website maintained by the Earth Observing Laboratory at NCAR (NCAR, 2022). The University of Wyoming Cloud Radar data is publicly available from the University of Wyoming (University of Wyoming 2023).

Acknowledgments
The authors thank Dr. Jon Rutz and two anonymous reviewers for their helpful comments that improved the quality of the paper. The authors thank the crew from the University of Wyoming King Air, particularly Dr. Samuel Haimov for their help in collecting the WCR data during the campaign. Funding for the UWKA was provided through the National Science Foundation (NSF) awards AGS-1361237 and AGS-1441831, respectively. Funding for Sarah Tessendorf was provided by Idaho Power Company. The research was supported under NSF Grants AGS-1546939, AGS-2016106. This material is based upon work supported by the National Center for Atmospheric Research (NCAR), which is a major facility sponsored by NSF under Cooperative Agreement 1852977.

References

Cann, M., & Friedrich, K. (2020). The role of moisture pathways on snowfall amount and distribution in the Payette Mountains of Idaho. *Monthly Weather Review*, *148*(5), 2033–2048. https://doi.org/10.1175/MWR-D-19-0350.1

Cao, Q., Shukla, S., DeFlorio, M. J., Ralph, F. M., & Lettenmaier, D. P. (2021). Evaluation of the sub-seasonal forecast skill of floods associated with atmospheric rivers in coastal western U.S. watersheds. *Journal of Hydrometeorology*, *22*(6), 1535–1552. https://doi.org/10.1175/JHM-D-20-0219.1

Colón-Robles, M., Rauber, R. M., & Jensen, J. B. (2006). Influence of low-level wind speed on droplet spectra near cloud base in trade wind cumulus. *Geophysical Research Letters*, *33*(20), L20814. https://doi.org/10.1029/2006GL027487

Dettinger, M. D., Ralph, F. R., Das, T., Neiman, P. J., & Cayan, D. R. (2011). Atmospheric rivers, floods, and the water resources of California. *Water*, *3*(2), 445–478. https://doi.org/10.3390/w3020445

Dominguez, F., Miguez-Macho, G., & Hu, H. (2016). WRF with water vapor tracers: A study of moisture sources for the North American monsoon. *Journal of Hydrometeorology*, *17*(7), 1915–1927. https://doi.org/10.1175/jhm-d-15-0221.1

Eiras Barca, J., Dominguez, F., Hu, H., Garaboa Paz, D., & Miguez-Macho, G. (2017). Evaluation of the moisture sources in two extreme landfalling atmospheric river events using an Eulerian WRF tracers tool. *Earth System Dynamics*, *8*(4), 1247–1261. https://doi.org/10.5194/esd-8-1247-2017

Gershunov, A., Shulgina, T., Clemesha, R. E. S., Guirguis, K., Pierce, D. W., Dettinger, M. D., et al. (2019). Precipitation regime change in western North America: The role of atmospheric rivers. *Scientific Reports*, *9*(1), 9944. https://doi.org/10.1038/s41598-019-46169-w

Guan, B., & Waliser, D. E. (2015). Detection of atmospheric rivers: Evaluation and application of an algorithm for global studies. *Journal of Geophysical Research: Atmospheres*, *120*(24), 12514–12535. https://doi.org/10.1002/2015JD024257

Hu, H., & Dominguez, F. (2019). Understanding the role of tropical moisture in atmospheric rivers. *Journal of Geophysical Research: Atmospheres*, *124*(13), 13826–13842. https://doi.org/10.1029/2019JD030867

Insua-Costa, D., & Miguez-Macho, G. (2018). A new moisture tagging capability in the Weather Research and Forecasting model: Formulation, validation, and application to the 2014 Great Lake-effect snowstorm. *Earth System Dynamics*, *9*, 167–185. https://doi.org/10.5194/esd-2017-80

Majewski, A., & French, J. (2020). Supercooled drizzle development in response to semi-coherent vertical velocity fluctuations within an orographic layer cloud. *Atmospheric Chemistry and Physics*, *20*(8), 5035–5054. https://doi.org/10.5194/acp-20-5035-2020

Miguez-Macho, G., Rios-Entraza, A., & Dominguez, F. (2013). *The impact of soil moisture and evapotranspiration fluxes on the spring water cycle in the Iberian Peninsula: A study with moisture tracers in WRF. 2013 Fall Meeting*. American Geophysical Union. Abstract H12B–05.

NCAR. (2022). NCAR [Dataset]. Retrieved from https://data.eol.ucar.edu/master_lists/generated/snowie/

NOAA. (2022). NOAA [Dataset]. Retrieved from https://psl.noaa.gov/psd2/coastal/satres/data/html/ardt_gfs.php

Ralph, F. M., Dettinger, M., Lavers, D., Gorodetskaya, I. V., Martin, A., Viale, M., et al. (2017). Atmospheric rivers emerge as a global science and applications focus. *Bulletin of the American Meteorological Society*, *98*(9), 1969–1973. https://doi.org/10.1175/BAMS-D-16-0262.1

Ralph, F. M., Rutz, J. J., Cordeira, J. M., Dettinger, M., Anderson, M., Reynolds, D., et al. (2019). A scale to characterize the strength and impacts of atmospheric rivers. *Bulletin of the American Meteorological Society*, *100*(2), 269–289. https://doi.org/10.1175/BAMS-D-18-0023.1

Rauber, R. M., Hu, H., Dominguez, F., Nesbitt, S. W., McFarquhar, G. M., Zaremba, T. J., & Finlon, J. A. (2020). Structure of an atmospheric river over Australia and the Southern Ocean. Part I: Tropical and midlatitude water vapor fluxes. *Journal of Geophysical Research: Atmospheres*, *125*(18), e2020JD032513. https://doi.org/10.1029/2020JD032513

Rutz, J. J., & Steenburgh, W. J. (2012). Quantifying the role of atmospheric rivers in the interior western United States. *Atmospheric Science Letters*, *13*(4), 257–261. https://doi.org/10.1002/asl.392

Rutz, J. J., Steenburgh, W. J., & Ralph, F. M. (2014). Climatological characteristics of atmospheric rivers and their inland penetration over the western United States. *Monthly Weather Review*, *142*(2), 905–921. https://doi.org/10.1175/MWR-D-13-00168.1

Rutz, J. J., Steenburgh, W. J., & Ralph, F. M. (2015). The inland penetration of atmospheric rivers over western North America: A Lagrangian analysis. *Monthly Weather Review*, *143*(5), 924–1944. https://doi.org/10.1175/MWR-D-14-00288.1

Shields, C. A., Rutz, J. J., Leung, L.-Y., Ralph, F. M., Wehner, M., Kawzenuk, B., et al. (2018). Atmospheric River Tracking Method Intercomparison Project (ARTMIP): Project goals and experimental design. *Geoscientific Model Development*, *11*(6), 2455–2474. https://doi.org/10.5194/gmd-11-2455-2018

Swales, D., Alexander, M., & Hughes, M. (2016). Examining moisture pathways and extreme precipitation in the U.S. Intermountain West using self-organizing maps. *Geophysical Research Letters*, *43*(4), 1727–1735. https://doi.org/10.1002/2015GL067478

Tessendorf, S. A., French, J. R., Friedrich, K., Geerts, B., Rauber, R. M., Rasmussen, R. M., et al. (2019). A transformational approach to winter orographic weather modification research: The SNOWIE project. *Bulletin of the American Meteorological Society*, *100*(1), 71–92. https://doi.org/10.1175/BAMS-D-17-0152.1

University of Wyoming - Research Flight Center. (2023). Wyoming Cloud Radar data from the University of Wyoming King Air during the University of Wyoming King Air during the Seeded and Natural Orographic Wintertime clouds-the Idaho Experiment (SNOWIE) project, Version 1.0. [Dataset]. University of Wyoming - Research Flight Center. https://doi.org/10.15786/M2CD4J

Waliser, D. E., & Guan, B. (2017). Extreme winds and precipitation during landfall of atmospheric rivers. *Nature Geoscience*, *10*(3), 179–183. https://doi.org/10.1038/ngeo2894

Zaremba, T. J., Heimes, K., Rauber, R. M., Geerts, B., French, J. R., Grasmick, C., et al. (2022). Vertical motions in orographic cloud systems over the Payette River Basin. Part II: Fixed and transient updrafts and their relationship to forcing. *Journal of Applied Meteorology and Climatology*, *61*(11), 1727–1745. https://doi.org/10.1175/JAMC-D-21-0229.1